nature materials

LETTERS

PUBLISHED ONLINE: 10 JANUARY 2012 | DOI: 10.1038/NMAT3207

Thermal conductivity of isotopically modified graphene

Shanshan Chen[1,2], Qingzhi Wu[2], Columbia Mishra[2], Junyong Kang[1], Hengji Zhang[3], Kyeongjae Cho[3,4], Weiwei Cai[1,2]*, Alexander A. Balandin[5]* and Rodney S. Ruoff[2]

In addition to its exotic electronic properties[1,2] graphene exhibits unusually high intrinsic thermal conductivity[3–6]. The physics of phonons—the main heat carriers in graphene—has been shown to be substantially different in two-dimensional (2D) crystals, such as graphene, from in three-dimensional (3D) graphite[7–10]. Here, we report our experimental study of the isotope effects on the thermal properties of graphene. Isotopically modified graphene containing various percentages of ^{13}C were synthesized by chemical vapour deposition (CVD). The regions of different isotopic compositions were parts of the same graphene sheet to ensure uniformity in material parameters. The thermal conductivity, *K*, of isotopically pure ^{12}C (0.01% ^{13}C) graphene determined by the optothermal Raman technique[3–7,10], was higher than 4,000 W mK^{-1} at the measured temperature $T_m \sim 320$ K, and more than a factor of two higher than the value of *K* in graphene sheets composed of a 50:50 mixture of ^{12}C and ^{13}C. The experimental data agree well with our molecular dynamics (MD) simulations, corrected for the long-wavelength phonon contributions by means of the Klemens model. The experimental results are expected to stimulate further studies aimed at a better understanding of thermal phenomena in 2D crystals.

Naturally occurring carbon materials are made up of two stable isotopes, ^{12}C (abundance ~ 99%) and ^{13}C (~1%). The change in isotope composition modifies the dynamic properties of the crystal lattices and affects their thermal conductivity, K. The isotopically purified materials are characterized by enhanced K (refs 11–13). The knowledge of the isotope effects on K is valuable for understanding the phonon transport. The isotope composition directly affects the phonon relaxation through phonon mass-difference scattering. The phonon-scattering rate on point defects, $1/\tau_P$, is given[14–16] as $1/\tau_P \propto V_0(\omega^\alpha/\upsilon^\beta)\Gamma$, where V_0 is the volume per atom in the crystal lattice, ω is the phonon frequency, υ is the phonon group velocity, Γ is the strength of the phonon–point defect scattering, and $\alpha = 3(4)$ and $\beta = 2(3)$ for a 2D(3D) system, respectively. In the perturbation theory Γ is written[14–16] as

$$\Gamma = \sum_i f_i \left[\left(1 - M_i/\overline{M}\right)^2 + \varepsilon \left(\gamma \left(1 - R_i/\overline{R}\right)\right)^2 \right] \qquad (1)$$

Here f_i is the fractional concentration of the substitutional foreign atoms, for example impurity, defect or isotope atoms, M_i is the mass of the ith substitutional atom, $\overline{M} = \sum_i f_i M_i$ is the average atomic mass, R_i is the Pauling ionic radius of the ith foreign atom, $\overline{R} = \sum_i f_i R_i$ is the average radius, γ is the Gruneisen parameter, which characterizes the anharmonicity of the lattice, and ε is a phenomenological parameter. The mass of a foreign atom (impurity, vacancy, defect or isotope) is known well whereas the local displacement $\Delta R = \overline{R} - R_i$ due to the atom radius or bond length difference is usually not known.

From kinetic transport theory, the thermal conductivity of graphene can be expressed as $K = (1/2)C\upsilon\Lambda$, where C is the specific heat capacity and Λ is the phonon mean free path (MFP). Assuming that Λ is limited by the anharmonic phonon Umklapp and point-defect scattering it can be written as $\Lambda^{-1} = \Lambda_U^{-1} + \Lambda_P^{-1}$, where $\Lambda = \upsilon\tau_U$ is the Umklapp-limited MFP, $\Lambda = \upsilon\tau_P$ is the point-defect-limited MFP, τ_U is the Umklapp-limited phonon lifetime, τ_P is the point-defect-limited phonon lifetime, which can be affected by isotopes, defects, impurities or vacancies. From these considerations and equation (1), one can see that the phonon-isotope scattering is unique in the sense that, unlike impurity or defect scattering, it involves only the well-defined mass-difference term, $\Delta M = \overline{M} - M_i$, without the ambiguous volume or bond-strength-difference term, $\Delta R = \overline{R} - R_i$ and ε.

As the system dimensionality changes from 3D to 2D, $1/\tau_P$ undergoes further modification owing to the different phonon density of states (DOS). The change in the phonon DOS reveals itself through the dependence of $1/\tau_P$ on ω and υ. Thus, the isotope effects in graphene are particularly important for understanding its thermal properties and, more generally, for the development of the theory of heat transport in low-dimensional systems. Until now, experimental studies of isotope effects in graphene have not been possible because of the unavailability of suitable samples. Theoretical studies of isotopically enriched graphene have just started[8,17] and experimental data is needed for model validation.

The samples used in this study were large-area high-quality monolayer graphene grown by CVD on the interior surfaces of Cu foil enclosures[18]. The characteristic grain size in our samples was determined to be over ~200 μm. To avoid potential sample-to-sample variation, we used the isotope-labelling technique[18,19] to synthesize single-layer graphene with regions of 0.01%, 1.1%, 50% and 99.2% of ^{13}C by turning on and off, sequentially, 99.99% $^{12}CH_4$, the 50:50 $^{12}CH_4/^{13}CH_4$ mixture, normal CH_4, and 99.2 % $^{13}CH_4$ gases. The isotope content in the localized graphene regions mirrored the dosing sequence employed. The isotope-modified regions were verified with micro-Raman spectroscopy using the distinctive

[1]Department of Physics, Fujian Key Laboratory of Semiconductor Materials and Application, Xiamen University, Xiamen 361005, China, [2]Department of Mechanical Engineering and the Materials Science and Engineering Program, University of Texas at Austin, Austin, Texas 78712, USA, [3]Department of Materials Science and Engineering and Department of Physics, University of Texas at Dallas, Richardson, Texas 75080, USA, [4]Division of WCU Multiscale Mechanical Design, School of Mechanical and Aerospace Engineering, Seoul National University, Seoul 151-742, Republic of Korea, [5]Department of Electrical Engineering and Materials Science and Engineering Program, University of California at Riverside, Riverside, California 92521, USA.
*e-mail: wwcai@xmu.edu.cn; balandin@ee.ucr.edu.

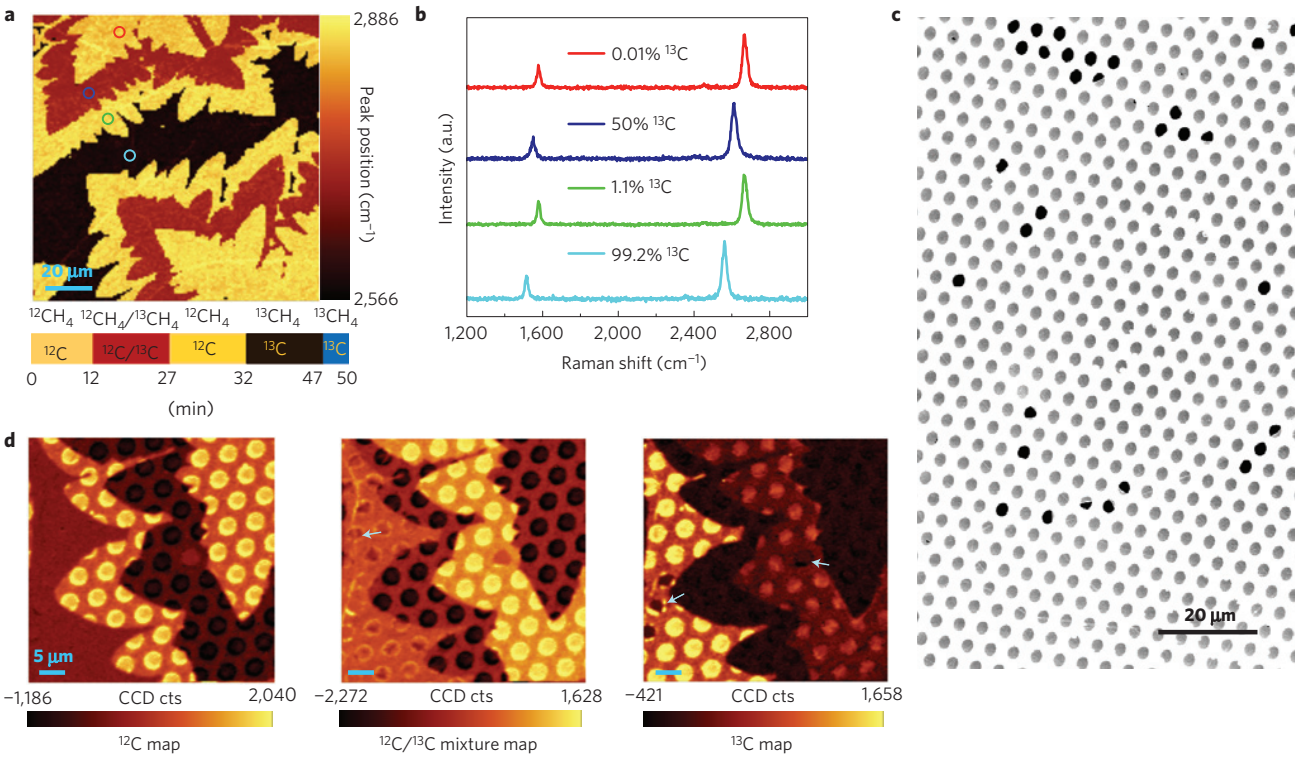

Figure 1 | Micro-Raman characteristics of the isotopically modified graphene. a, Raman map (2,530 ~ 2,730 cm^{-1}) of the 2D bands. The colour bar shown below indicates the dosing sequence for the four regions. **b**, Raman spectra of graphene measured at the positions labelled by the coloured circles in **a**. **c**, SEM image of graphene transferred onto the SiN_x holey membrane. **d**, Raman maps of graphene transferred onto the SiN_x holey membrane. From left to right, three Raman maps showing the integrated intensity of the 2D band of 0.01% ^{13}C (2,630 ~ 2,730 cm^{-1}), the 50:50 $^{12}C/^{13}C$ mixture (2,560 ~ 2,660 cm^{-1}) and 99.2% ^{13}C (2,530 ~ 2,630 cm^{-1}) graphene, respectively. The *x*-axis shows counts (cts) from the CCD (charge-coupled device). The arrows indicate wrinkles and cracks in some samples, which were excluded from the thermal measurements.

phonon mode signatures of the isotope-engineered materials[18–20]. The graphene samples were transferred to a Au-coated silicon nitride (SiN_x) membrane with a pre-fabricated 100 × 100 array of 2.8-μm-diameter holes. A part of the same graphene film was transferred to a Si wafer with a 285-nm-thick SiO_2 layer[21]. Details of the isotope-engineered graphene preparation can be found in the Methods section.

Raman spectroscopy of graphene transferred to the 285-nm SiO_2/Si wafer was performed under 532-nm laser light excitation (Fig. 1). The distinctive Raman peaks for different $^{12}C/^{13}C$ ratios allow an accurate mapping of the isotopically labelled graphene regions[18,19]. The Raman 2D-band position map over a 120 × 120 μm^2 area shows a 'six-lobe' shape with growing edges that resemble dendrites consistent with our previous observations[18]. Figure 1a is the Raman peak position mapping (2,530 ~ 2,730 cm^{-1}) of four regions with different ^{13}C-isotope contents. The colour bar at the bottom indicates the dose sequence. The G-peak and 2D-band positions in Raman spectra of graphene with 0.01%, 50%, 1.1%, and 99.2% ^{13}C-isotope content are presented in Fig. 1b. They are recorded from the different sample spots marked by the corresponding coloured circles in Figure 1a. The frequency ω of the optical phonon at the Brillouin-zone centre varies with the atomic mass, M, as $\omega \propto M^{-1/2}$, making the Raman shift for ^{13}C approximately $(12/13)^{-1/2}$ times smaller than that for ^{12}C (refs 22–24). The latter explains the observed sequence of Raman peak positions in Fig. 1b. The experimental difference between the lowest 99.2% ^{13}C peak and the highest 0.01% ^{13}C peak is ~64 cm^{-1}, which is in agreement with the theory and attests for the high quality of our isotopically modified graphene.

A different portion of the same ^{13}C-labelled monolayer graphene sheet was transferred onto a Au-coated SiN_x holey membrane. Figure 1c shows a scanning electron microscopy (SEM, FEI Quanta-600) image of graphene on the SiN_x holey membrane. For a few holes in the array the graphene film is broken or wrinkled. Before the thermal measurements, Raman mapping with a laser power of ~8 mW (on the sample surface) was carried out on the selected graphene areas, which could heat the graphene membranes up to about 600 K. The procedure was implemented both to further remove the PMMA residue and to verify the ^{13}C concentration in the suspended graphene membranes. All portions of the sample were subjected to the same treatment.

Figure 1d shows 40 × 40 μm^2 integrated intensity Raman maps of the 2D-band of the ^{12}C (2,630 ~ 2,730 cm^{-1}), the 50:50 $^{12}C/^{13}C$ mixture (2,560 ~ 2,660 cm^{-1}) and the ^{13}C (2,530 ~ 2,630 cm^{-1}), respectively. The bright region in the ^{12}C-map from right-to-left corresponds to 0.01% ^{13}C graphene grown at the beginning and 1.1% ^{13}C grown at the third dosing sequence. The bright region in the $^{12}C/^{13}C$-mixture map and ^{13}C-map corresponds to 50% ^{13}C and 99.2% ^{13}C graphene grown in the second and last dosing sequence, respectively. Raman mapping was used to avoid parts of the sample with wrinkles and cracks[18,19]. The arrow in the $^{12}C/^{13}C$-mixture map shows a wrinkle in the suspended graphene film and the arrows in the ^{13}C map indicate places where graphene either does not cover or only partially covers the holes in the SiN_x membrane (Fig. 1d).

The thermal conductivity, K, of the suspended isotopically modified graphene layers was measured using the non-contact optothermal Raman technique[3–7,10,25]. Details of the measurements are provided in the Supplementary Information. Typical results for K as a function of the measured temperature T_m (extracted from the Raman data) for four regions with different isotope composition are plotted in Fig. 2. The isotopically pure graphene (0.01% ^{13}C) has the highest K ~4,120 ± 1,410 W mK^{-1} at T_m ~ 320 K. For comparison,

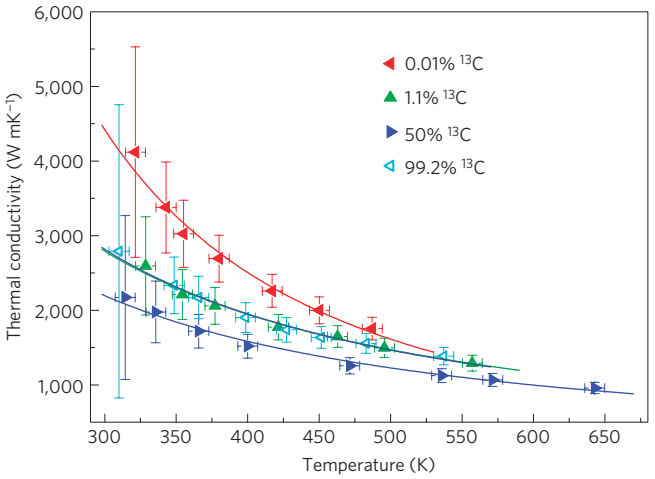

Figure 2 | Thermal conductivity *K* of the suspended graphene film with ^{13}C isotope concentrations of 0.01%, 1.1% (natural abundance), 50% and 99.2%, respectively, as a function of the temperature measured with the micro-Raman spectrometer. The solid lines are a guide to the eye only. The experimental errors were estimated by means of the square-root-sum error propagation approach, including the following error sources: the Raman peak position calibration, temperature resolution of the Raman measurement method, and the uncertainty of the laser absorption.

the layer of the natural abundance graphene (^{13}C 1.1%) of the same size has $K \approx 2{,}600 \pm 658$ W mK^{-1} at $T_m \sim 330$ K. The near-room-temperature K for the natural abundance graphene is within experimental uncertainty consistent with previous studies[3–7,10]. Graphene with ^{13}C-content increased to 99.2% has a similar K to the natural abundance graphene. The latter is explained by the fact that in both cases the fraction of 'isotope impurities', which give rise to the phonon mass-difference scattering (see equation (1)), is about the same ~1% of the total carbon atoms. The extrapolated K values at 300 K are 4,419 W mK^{-1}, 2,792 W mK^{-1}, 2,197 W mK^{-1} and 2,816 W mK^{-1} for 0.01% ^{13}C ('isotopically pure ^{12}C'), 1.1% ^{13}C (natural graphene), 50% ^{13}C ('isotopically disordered' graphene), and 99.2% ^{13}C (^{13}C-enriched graphene), respectively. When compared at the same temperature, K is enhanced by ~58% in the isotopically pure ^{12}C graphene with respect to natural graphene near room temperature.

One can see from Fig. 2 that the lowest K is observed in graphene characterized by the strongest mixture of the isotopes (50% ^{13}C), as expected from equation (1). The evolution of K with the isotope content is mostly produced by changes in the phonon–point defect scattering rate $1/\tau_P$ through the mass-difference term $\Delta M = \overline{M} - M_i$. The phonon υ and mass density do not undergo substantial modification through the isotope composition. The relative change in the phonon velocity $\upsilon_{^{12}C}/\upsilon_{natural}$ is related to the mass densities of the respective lattices $\upsilon_{^{12}C}/\upsilon_{natural} = (M_{natural}/M_{^{12}C})^{1/2}$. Removal of 1% ^{13}C in natural diamond causes the velocity to increase only by a factor of 1.0004 (ref. 13), which can not account for the observed ~58% change in K.

To verify the reproducibility and minimize the data uncertainty, we prepared 16, 21, 21 and 22 suspended graphene membranes with 0.01%, 1.1%, 50% and 99.2% ^{13}C regions, respectively. Special care was given to select samples without grain boundaries, wrinkles or cracks. The measurement statistics at $T_m \sim 380$ K is presented in Fig. 3a (see also Supplementary Information). The solid lines in Fig. 3a, fitted by the normal distribution, give an approximately 10% variance of K. The data scatter was mainly attributed to the variation in the optical absorption from membrane to membrane and the uncertainty of measurement of T with the Raman spectrometer[10]. The average K at $T_m \approx 380$ K as a function of ^{13}C concentration is plotted in Fig. 3b. The 0.01% ^{13}C graphene had the highest average K of 2,805 W mK^{-1}, which is 36% higher than natural abundance graphene (1.1% ^{13}C) and 77% higher than 50% ^{13}C. The room-temperature K values are correspondingly higher

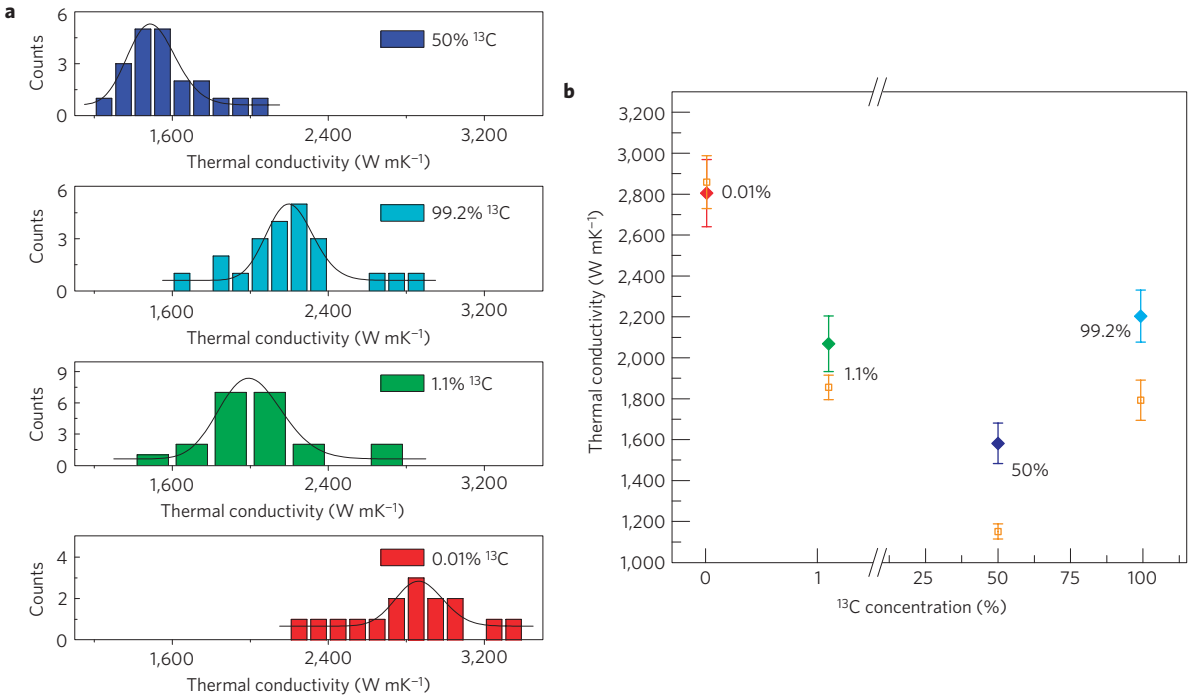

Figure 3 | Thermal conductivity of graphene as a function of its isotopic composition. a, Histograms of K for graphene films with 0.01%, 1.1%, 50% and 99.2% ^{13}C isotopic concentration at ~380 K. The solid lines represent fits to the experimental data with the normal distribution. **b**, The average value of the measured thermal conductivity K as a function of ^{13}C concentration at ~380 K. The MD simulations results for K are shown as yellow squares for comparison.

for all isotopic compositions. The maximum difference at room temperature is ~100% between K of 0.01% ^{13}C and that of 50% $^{13}C/^{12}C$-mixture graphene.

Recently, MD simulations were used to compute the isotope effect on K of graphene[26]. The simulations predicted enhanced K for isotopically pure ^{12}C or ^{13}C graphene and strongly reduced K for mixed isotope graphene even with a small (~ 1%) addition of foreign isotopes. The MD models account well for the contributions of the short-wavelength phonons but omit the long-wavelength phonons, which are important for heat transport in graphene[8,9,14–16]. We modified a previous simulation approach by adding the long-wavelength phonon contributions from the Klemens model[14,15]. The MD treatment of the short-wavelength phonons is essential for accurately describing the isotope scattering effects and the Klemens correction allows one to obtain K values for the large graphene samples (Supplementary Information). We used the optimized Brenner potential, also referred to as the reactive empirical bond order potential (REBO; ref. 26). It was shown from the solution of the Boltzmann transport equation (BTE) that the optimized Tersoff and Brenner potentials yield similar thermal conductivity values for graphene[27].

At $T \sim 380$ K, we obtained the following K from MD simulations (Fig. 3b): $2{,}859 \pm 129$ W mK^{-1}, $1{,}855 \pm 60$ W mK^{-1} and $1{,}151 \pm 38$ W mK^{-1} for isotopically pure ^{12}C, 99% ^{12}C (1% ^{13}C) and 50% $^{13}C/^{12}C$-mixture graphene, respectively. According to our MD simulations with the Klemens correction for the long-wavelength phonons, K of the isotopically pure ^{12}C graphene was enhanced by ~40% relative to the natural graphene, which is in line with our measurements. Some discrepancy may be related to the wave interference effects characteristic for materials with large isotope impurity concentrations (>10%; ref. 28). The uncertainties of MD simulations (below 5%) indicated in Fig. 3b were obtained from the Green–Kubo method, where K is computed by averaging the integral of the heat current autocorrelation function from ten uncorrelated micro-canonical ensembles. The error bars characterize the fluctuation of the averaged thermal conductivity value. It was also predicted theoretically that further reduction in K could be achieved if the isotopes were organized in small-sized clusters rather than being distributed randomly[29].

We have also compared our experimental results and MD simulations for the natural abundance (1.1% ^{13}C) graphene with the predictions of the BTE models[8,9]. Plugging in $T = 380$ K and a characteristic size $L = 2.8\,\mu$m to both numerical[8] and semi-analytical[9] models, we obtained $K \sim 2{,}000$ W mK^{-1} (with $\gamma_{LA} = 1.8$ and $\gamma_{TA} = 0.75$ as Gruneisen parameters for the longitudinal and transverse phonon modes in the semi-analytic model). This value is in quantitative agreement with the experimental and MD data points shown in Fig. 3b.

It is interesting to note that the trend for K as a function of ^{13}C concentration is in line with the predictions of the well-established virtual crystal model[30] used to calculate K in alloy semiconductors such as Si_xGe_{1-x}, $Al_xGa_{1-x}As$ or $Al_xGa_{1-x}N$. This model predicts the highest K for the material with either $x \sim 0$ or $(1-x) \sim 0$ and a fast decrease to a minimum as x deviates from 0. The fact that, unlike in semiconductor compounds, the phonon-point defect scattering in the isotopically modified graphene is limited to the mass-difference term (equation (1)) increases the value of the experimental data obtained for theory development.

Methods

Preparation of isotopically-engineered graphene. Graphene films were grown on 25-μm thick Cu foils (Alfa Aesar) by a CVD method in a hot wall tube furnace at temperatures up to 1,035 °C using a mixture of methane and hydrogen, similar to the method reported previously (Supplementary Information). The carbon isotope labelling[19] and the copper-foil enclosure[18] technique have been employed to synthesize large-grain-size monolayer graphene with regions of 0.01%, 1.1%, 50%, or 99.2% ^{13}C on the same graphene sheet. The hydrogen flow rate was kept constant at 2 standard cubic centimetres per minute with a partial pressure of 27 mtorr. The chamber background pressure was 17 mtorr. The methane flow rate was held at 1 standard cubic centimetres per minute with the following dosing sequence: (1) 12 min for 99.99% $^{12}CH_4$ (Cambridge Isotopes); (2) 15 min for 50: 50 $^{12}CH_4/^{13}CH_4$ mixture; (3) 15 min for 98.9% $^{12}CH_4$ (Air Gas); (4) 15 min for 99.2% $^{13}CH_4$ (Cambridge Isotopes); (5) 3 min for 99.2% $^{13}CH_4$ (Cambridge Isotopes). The partial pressure from step 1 to 4 was approximately 36 mtorr, and a much higher partial pressure of 1 torr was set for step 5 so as to fill the gaps between graphene domains and form a fully covered graphene layer on the surfaces on the inside of the enclosure[2]. The graphene-coated Cu foil enclosure was then carefully unfolded to expose what had been the inner surface (that is, what had been the surface inside the 'pocket'), as this surface has a particularly large grain size[18]. The details of the graphene transfer procedure are provided in the Supplementary Information.

Received 10 June 2011; accepted 21 November 2011; published online 10 January 2012

References

1. Novoselov, K. S. *et al.* Two-dimensional gas of massless Dirac fermions in graphene. *Nature* **438,** 197–200 (2005).
2. Zhang, Y. B., Tan, Y. W., Stormer, H. L. & Kim, P. Experimental observation of the quantum Hall effect and Berry's phase in graphene. *Nature* **438,** 201–204 (2005).
3. Balandin, A. A. *et al.* Superior thermal conductivity of single layer graphene. *Nano Lett.* **8,** 902–907 (2008).
4. Ghosh, S. *et al.* Extremely high thermal conductivity in graphene: Prospects for thermal management application in nanoelectronic circuits. *Appl. Phys. Lett.* **92,** 151911 (2008).
5. Cai, W. *et al.* Thermal transport in suspended and supported monolayer graphene grown by chemical vapor deposition. *Nano Lett.* **10,** 1645–1651 (2010).
6. Chen, S. *et al.* Raman measurement of thermal transport in suspended monolayer graphene of variable sizes in vacuum and gaseous environments. *ACS Nano* **5,** 321–328 (2011).
7. Ghosh, S. *et al.* Dimensional crossover of thermal transport in few-layer graphene. *Nature Mater.* **9,** 555–558 (2010).
8. Nika, D. L., Pokatilov, E. P., Askerov, A. S. & Balandin, A. A. Phonon thermal conduction in graphene: Role of Umklapp and edge roughness scattering. *Phys. Rev. B* **79,** 155413 (2009).
9. Nika, D. L., Ghosh, S., Pokatilov, E. P. & Balandin, A. A. Lattice thermal conductivity of graphene flakes: Comparison and bulk graphite. *Appl. Phys. Lett.* **94,** 203103 (2009).
10. Balandin, A. A. Thermal properties of graphene and nanostructured carbon materials. *Nature Mater.* **10,** 569–581 (2011).
11. Wei, L., Kuo, P. K., Thomas, R. L., Anthony, T. R. & Banholzer, W. F. Thermal diffusivity of isotopically modified single crystal diamond. *Phys. Rev. Lett.* **70,** 3764–3767 (1993).
12. Anthony, T. R. *et al.* Thermal diffusivity of isotopically enriched ^{12}C diamond. *Phys. Rev. B* **42,** 1104–1111 (1990).
13. Bray, J. W. & Anthony, T. R. On the thermal conductivity of diamond under changes of its isotopic character. *Z. Phys. B* **84,** 51–57 (1991).
14. Klemens, P. G. & Pedraza, D. F. Thermal conductivity of graphite in the basal plane. *Carbon* **32,** 735–741 (1994).
15. Klemens, P. G. Theory of the A-plane thermal conductivity of graphene. *J. Wide Bandgap Mater.* **7,** 332–339 (2000).
16. Klemens, P. G. The scattering of low-frequency lattice waves by static imperfections. *Proc. Phys. Soc. A* **68,** 1113–1128 (1955).
17. Jiang, J. W., Lan, J. H., Wang, J. S. & Li, B. W. Isotopic effects on the thermal conductivity of graphene nanoribbons: Localization mechanism. *J. Appl. Phys.* **107,** 054314 (2010).
18. Li, X. S. *et al.* Large area graphene single crystals grown by low pressure chemical vapor deposition of methane on copper. *J. Am. Chem. Soc.* **133,** 2816–2819 (2011).
19. Li, X. S., Cai, W. W., Colombo, L. & Ruoff, R. S. Evolution of graphene growth on Ni and Cu by carbon isotope labeling. *Nano Lett.* **9,** 4268–4272 (2009).
20. Li, X. S. *et al.* Graphene films with large domain size by a two-step chemical vapor deposition process. *Nano Lett.* **10,** 4328–4334 (2010).
21. Li, X. S. *et al.* Transfer of large-area graphene films for high-performance transparent conductive electrodes. *Nano Lett.* **9,** 4359–4363 (2009).
22. Ager, J. W & Haller, E. E. Isotopically engineered semiconductors: From bulk to nanostructures. *Phys. Status Solidi. A* **203,** 3550–3558 (2006).
23. Ramirez, A. P. *et al.* Isotope effects in superconducting Rb_3C_{60}. *Phys. Rev. Lett.* **68,** 1058–1060 (1992).
24. Miyauchi, Y. & Maruyama, S. Identification of an excitonic phonon sideband by photoluminescence spectroscopy of single-walled carbon-13 nanotubes. *Phys. Rev. B* **74,** 035415 (2006).
25. Seol, J. H. *et al.* Two-dimensional phonon transport in supported graphene. *Science* **328,** 213–216 (2010).

26. Zhang, H., Lee, G., Fonseca, A. F., Borders, T. L. & Cho, K. Isotope effect on the thermal conductivity of graphene. *J. Nanomater.* **2010,** 537657 (2010).
27. Lindsay, L. & Broido, D. A. Optimized Tersoff and Brenner empirical potential parameters for lattice dynamics and phonon thermal transport in carbon nanotubes and graphene. *Phys. Rev. B* **81,** 205441 (2010).
28. Savic, I., Mingo, N. & Stewart, D. A. Phonon transport in isotope-disordered carbon and boron-nitride nanotubes: Is localization observable? *Phys. Rev. Lett.* **101,** 165502 (2008).
29. Mingo, N., Esfarjani, K., Broido, D. A. & Stewart, D. A. Cluster scattering effects on phonon conduction in graphene. *Phys. Rev. B* **81,** 045408 (2010).
30. Abeles, B. Lattice thermal conductivity of disordered semiconductor alloys at high temperatures. *Phys. Rev.* **131,** 1906–1911 (1963).

Acknowledgements

The authors appreciate comments by L. Shi and H. Zhao. The work at UTA was supported by the National Science Foundation grant no. 1006350, the W. M. Keck Foundation, and the Office of Naval Research. The work at XMU was supported by the National Natural Science Foundation of China through grant nos. 91123009, 111104228, 10975115, 60827004 and 90921002 and the '973' program 2012CB619301 and 2011CB925600. The work at UCR was supported, in part, by the Semiconductor Research Corporation—Defense Advanced Research Project Agency FCRP Functional Engineered Nano Architectonic centre, National Science Foundation and US Office of Naval Research. K.C. was supported by the NRF of Korea through WCU program grant no. R-31-2008-000-10083-0. R.S.R. acknowledges the support of the W.M. Keck Foundation.

Author contributions

R.S.R. coordinated the project and data analysis; A.A.B. led the thermal data analysis; S.C. performed sample growth, measurements and data analysis; W.C. carried out the Raman optothermal measurement and data analysis. Q.W. assisted on the sample transfer. C.M. and J.K. contributed to the discussion of the data analysis. H.Z. and K.C. performed MD simulations; S.C., W.C., R.S.R. and A.A.B. wrote the manuscript.

Additional information

The authors declare no competing financial interests. Supplementary information accompanies this paper on www.nature.com/naturematerials. Reprints and permissions information is available online at http://www.nature.com/reprints. Correspondence and requests for materials should be addressed to W.C. or A.A.B.